Monatsh Chem (2015) 146:883–890
DOI 10.1007/s00706-014-1363-x

ORIGINAL PAPER

A computational study of platinum adsorption on defective and non-defective silicon carbide nanotubes

Farzad Molani · Seifollah Jalili · Jeremy Schofield

Received: 31 August 2014 / Accepted: 19 November 2014 / Published online: 20 December 2014

Abstract Platinum adsorption on the pristine, Stone–Wales defect, and vacancy defects sites in (8,0) zigzag silicon carbide nanotubes are studied based on the spin-polarized density functional theory. The formation of the Stone–Wales defects with the axial bond rotation is more favorable than the circumferential one. In addition, the vacancy of the carbon atom is more desirable than the silicon atom. The stable adsorption sites and their binding energies on different defect types are analyzed and compared to those on the perfect side wall. It is determined that the adsorption of Pt atom on nine-membered ring in carbon vacancy defect is the most exothermic site. Thus, the presence of intrinsic defects can enhance the reactivity of silicon carbide nanotubes toward Pt atom. Furthermore, the dangling bonds are the main driving force in preventing Pt atom from clustering. It is noticeable that the systems with Pt atom remained semiconductor with direct band gaps. Pt atom on pristine and vacancy-defective silicon carbide nanotubes were positively charged, whereas on Stone–Wales structures, Pt atom gained some charge. In addition, only silicon vacancy structure as structure without Pt atom showed ferromagnetic ordering, while all the systems in presence of Pt atom exhibited non-magnetic moment.

Keywords Density functional theory · Electronic structure · Silicon carbide nanotube · Platinum · Defect

F. Molani (✉)
Department of Chemistry, Sanandaj Branch, Islamic Azad University, P.O. Box 618, Sanandaj, Iran
e-mail: f.molani@iausdj.ac.ir

S. Jalili
Department of Chemistry, K. N. Toosi University of Technology, P.O. Box 15875-4416, Tehran, Iran

S. Jalili
Computational Physical Sciences Research Laboratory, School of Nano-Science, Institute for Research in Fundamental Sciences (IPM), P.O. Box 19395-5531, Tehran, Iran

J. Schofield
Department of Chemistry, Chemical Physics Theory Group, University of Toronto, 80 Saint George Street, Toronto, ON M5S 3H6, Canada

Introduction

Among recently created nanomaterials, silicon carbide nanostructures have attracted great attention because of their many potential applications in field emission such as, thermal stability, high thermal conductivity, hydrogen storage, gas sensing, transition metal adsorption, and extreme hardness [1–6]. Lately, silicon carbide nanotubes (SiCNTs) have been successfully synthesized with a silicon (Si) to carbon (C) ratio of 1:1 via the reaction of Si with multi-walled carbon nanotubes (CNTs) [7]. Unlike CNTs, SiCNTs regardless of chirality are semiconductors [2, 4]. The vacancy defects (incomplete bonding defects) and the Stone–Wales (SW) defect [8] (a typical topological defect in the carbon nanostructures which comprises two pairs of five-membered and seven-membered rings) have been extensively studied in CNTs [9–11], boron nitride nanotube (BNNTs) [12], BC_3 nanotubes [13], C_3N nanotube (C_3NNT) [14], and SiCNT [15–17].

Recently, some work has done on coating CNTs, boron carbonitride nanotubes, and BNNTs using transition metals (TMs) [18–21]. Also, theoretical simulations have been reported that many interesting physical and electronic properties of a series of TMs can be chemically adsorbed on the outer surface of SiCNTs [5, 6, 22]. Furthermore,

Wang and Liew have shown that the interactions between atomic Li with SW defective SiCNTs are larger than the pristine one [16].

Pt-coated CNTs and BNNT have already attracted research interest because they are good catalysts, potential gas sensors, and hydrogen storage materials [23–28]. Based on density functional theory (DFT) calculations, theoretical studies have shown that the Pt atom has a larger binding with defective CNT [29, 30] and BNNT [23] in comparison with non-defective nanotubes. According to the above discussions, we believe that investigation of adsorption of atomic Pt on the pristine and defective SiCNT seems to be necessary.

Based on our knowledge, no prior theoretical and experimental investigations have been reported for the effect of defects on adsorption of Pt atom on (8,0) SiCNT. In this paper, we report the first ab initio density functional theory (DFT) study of structural, electronic, and magnetic properties of defected SiCNTs coated with Pt atom.

Results and discussion

Pristine and defective SiCNT

Full geometry optimization of zigzag (8,0) SiCNT is performed without any constraints, as depicted in Fig. 1. The calculated Si–C bond length and average diameter of nanotube are about 1.80 and 7.9 Å, respectively. These values are in good agreement with previous studies [6, 31]. Three kinds of defective SiCNT are chosen to study and interact with the single Pt atom and compared with the adsorption on perfect tubes. These structures include SW defect, single vacancy of Si atom (Si_V), and single vacancy of C atom (C_V).

Optimized structures for SiCNT contain a SW defect are shown in Fig. 1. As a result of bond rotation by 90°, there are two kinds of SW defects for a zigzag SiCNT. Figure 1b, c show the fully optimized configurations of SWs, labeled as SW-a (rotating an axial Si–C bond) and SW-c (rotating a circumferential Si–C bond). The local structure around the defected site for both kinds of SW defects in SiCNT is compared with those of the pristine nanotube in Table 1. As a result, the tube diameter near the defect position increases by ~0.7 Å and decreases by ~1 Å for axial and circumferential bond rotation, respectively. The data listed in Table 1 reveal that the length of the central bond (the bond between atoms 1 and 2 in Fig. 1) for SW defect structures is considerably shorter than the corresponding bond of the pristine structure. The same behavior is also observed for CNT [9, 32], BNNT [9], and C_3NNT [14]. It is also worth mentioning that the length of the central bond in SW-c structure is shorter than the SW-a structure which is exactly similar to that reported in the CNT [9, 32], BNNT [33], and C_3NNT [14]. The calculated θ_p values for both atoms 1 and 2 in Fig. 1, as compared to the values for the pristine tube, are presented in Table 1. It has been shown that, the magnitude of θ_p has been correlated with the local reactivity of atomic sites on the CNTs [11, 34, 35]. In defective region, the results showed that θ_p for C atom and Si atom decreases and increases, respectively. Further, carbon's θ_p in SW-c nanotube decreases more than SW-a nanotube with respect to the perfect one, while SW-c of Si atom has the highest θ_p compared with SW-a and non-defective nanotube. As presented in Table 1, atoms with positive charge variation have higher θ_p. Furthermore, atoms with the highest θ_p can increase the bond length (steric hindrance). Moreover, Si atom in 7-7 ring fusion in SW-c structure move outward more than C atom due to steric effects. Unlike SW-a, reactive site in SW-c structure is localized on 7-7 ring fusion. Therefore, in SW-c structure, 7-7 ring fusion could count as are active site.

As Table 1 shows the formation energies for SW defects are defined as:

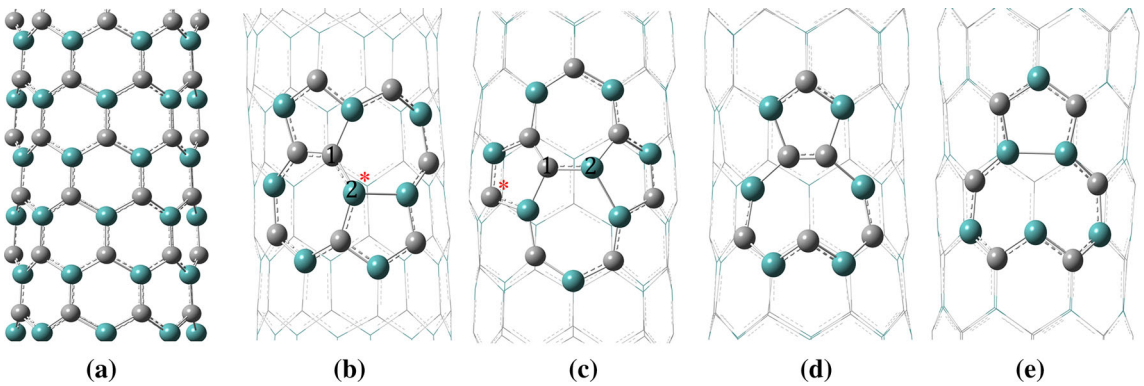

Fig. 1 Optimized structures of **a** perfect (8,0) SiCNT, **b** SW-c, **c** SW-a, **d** Si_V, and **e** C_V structures. Atoms with the highest pyramidalization angle are shown by *asterisks*. *Gray* and *dark turquoise colors* represent carbon and silicon atoms, respectively (color figure online)

Table 1 Structural and electronic properties of perfect and SW defects of SiCNT with and without Pt atom

System	Perfect	SW-a	SW-c	Pt@perfect	Pt@SW-a	Pt@SW-c
Central bond length/Å	–	1.779	1.754	–	1.801	1.786
d_{min} (Pt–Si)/Å	–	–	–	2.45	2.22	2.34
d_{min} (Pt–C)/Å	–	–	–	2.04	3.4	2.96
θ_p for 1, 2 atoms/deg	9.41, 3.29	7.39, 12.88	4.35, 14.20	2.46, 9.56	8.20, 16.67	5.37, 8.11
Total magnetization/μ_B	0.00	0.00	0.00	0.00	0.00	0.00
Formation energy/eV	–	2.75	2.99	–	–	–
Binding energy/eV				−3.88	−5.65	−5.61
Charge variation for Pt atom/e	–	–	–	−0.1	0.1	0.03
Charge variation for 1, 2 atoms/e	–	−0.52, 0.45	−0.49, 0.52	−0.15, 0.1	−0.55, 0.37	−0.58, 0.42
Energy gap/eV	1.21	0.85	0.66	1.00	0.73	0.8

Table 2 Structural and electronic properties of perfect and vacancy defects of SiCNT in presence and not of Pt atom

System	C_V	Si_V	Pt@C_V	Pt@Si_V
Length of new bonds/Å	2.314 (Si–Si)	1.410 (C–C)	2.48 (Si–Si)	1.49 (C–C)
d_{min} (Pt–Si)/Å	–	–	2.24	2.52
d_{min} (Pt–C)/Å	–	–	3.50	1.96
Total magnetization/μ_B	0.00	1.60	0.00	0.00
Formation energy/eV	2.24	5.36	–	–
Binding energy/eV	–	–	−6.66	−5.85
Charge variation for Pt atom/e	–	–	−0.08	−0.38
Charge variation for under-coordinated atom/e	0.48	−0.38	−0.17	0.15
Energy gap/eV	1.05	0.87[a], 0.32[b]	1.15	0.54

[a,b] Spin-up and spin-down, respectively

$$E_f = E_{SW} - E_{pristine},$$

where $E_{pristine}$ and E_{SW} are the total energies of a pristine SiCNT and SiCNT with SW defect, respectively. The positive formation energy means that the formation of these defects in SiCNT is an endothermic process. The bond rotations in SiCNT, like CNTs [9, 32], BNNTs [33], and C_3NNT [14] have positive formation energies. The axial bond rotation is more stable than the circumferential one which is in agreement with the results published by Wang et al. [15].

When a single atom is removed from the SiCNT sidewall, unconstrained structure optimization leads to the formation of a new bond. This bond is perpendicular to the tube axis and the system is reconstructed to a five-membered ring and a nine-membered ring with an under-coordinated atom (UA) around the local defective region, as demonstrated in Fig. 1d, e. As denoted in Table 2, the new bond in defected C_V is longer than of the Si_V defect. In addition, the unsaturated C atom in Si_V defect is more outward than the unsaturated Si atom in C_V defect as a result of charge variation on UA. For vacancies, defect formation energy is calculated from the energies of defected and pristine structures by:

$$E_f = E_{defected} + \mu_X - E_{pristine},$$

where μ_X is the chemical potential of carbon in a bulk graphene or silicon in zinc-blend structure. One reason for positive defect formation energy is that the UA remained after the reconstruction. The results showed that C_V defect has 3.12 eV formation energy lower than Si_V defect.

The electronic band structures and density of state (DOS) of the pristine and defective SiCNT are displayed in Figs. 2 and 3. Moreover, the values of the energy gap are listed in Tables 1 and 2. It should be considered that defective structures remain semiconductor with a direct band gap. The energy gap for the pristine nanotube is 1.21 eV which is in agreement with previous results [6, 31]. The SW defects reduce the energy gap. In addition, structure with a circumferential bond rotation has a lower energy gap in comparison with the structures with an axial one. As depicted in Figs. 2b, c and 3b, c, one "defected state" is observed near valance bands maximum (VBM) in band structures. The Fermi level shifts up to the conduction band minimum (CBM) when SW-c defect occurred, meanwhile in SW-a structure the Fermi level shifts down to VBM. Based on spin-polarized calculations, different electronic properties are obtained for spin-up and spin-down in Si_V structure.

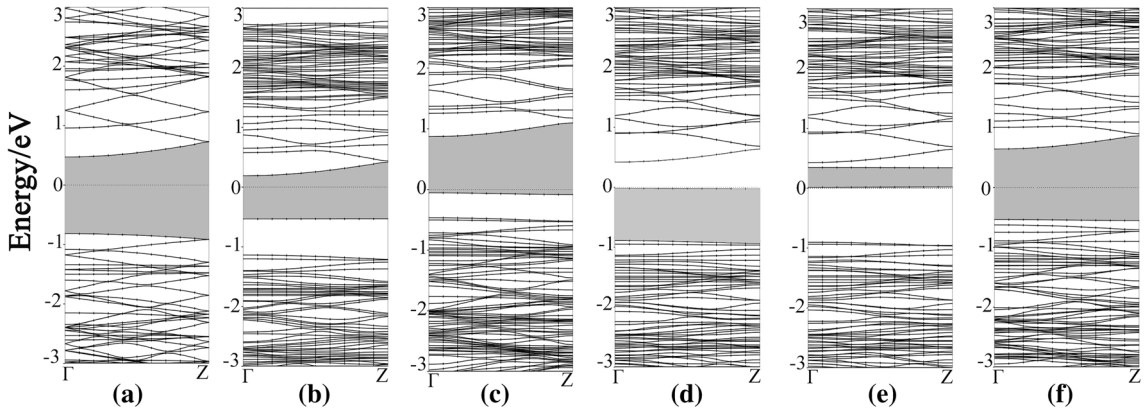

Fig. 2 Electronic band structure of **a** perfect, **b** SW-c, **c** SW-a, **d** spin-up for Si_V, **e** spin-down for Si_V, and **f** C_V. The gap between valence and conduction bands is distinguished by *gray color*

A silicon vacancy introduces two "defected states" within the band gap for both spin-up and spin-down channels (see Figs. 2d, e, 3d). Moreover, upon C atom removal, a "defected state" is introduced in the gap region near the top of the VBM (see Figs. 2f, 3e). In the defective structures, the energy levels of VBM become quite flat and show more obvious energy level localization, compared with pure SiCNT. Generally, the band gap decreases from 1.21 eV (perfect SiCNT) to 0.85 eV (SW-a defect), 0.63 eV (SW-c defect), 0.32 eV (Si_V defect), and 1.05 eV (C_V defect).

The net magnetic moments for perfect and defective structures are also listed in Tables 1 and 2. The structures with SW and C_V defects remain paramagnetic ordering. Moreover, the Si_V structure has net magnetic moment of 1.6 μ_B. The calculated charge variations (ΔQ) of UA for the vacant defected systems are obtained by Löwd in charge analysis (Table 2). It is noteworthy that a positive value for ΔQ indicated that the UA gained electron density. In Si_V (C_V) structure, UA connected to two Si(C) atoms instead of three atoms. Due to electronegativity differences between C and Si atoms, the UA in Si_V and C_V lost and got some charge, respectively.

Atomic Pt adsorption on the surface of a perfect and defective (8,0) SiCNT

Several different adsorption sites are selected for the Pt atom on the perfect SiCNTs: directly above an Si atom (Si), above a C atom (C), over an axial SiC bond (BA), over a circumferential Si–C bond (BC), and above a hexagon center (H). After full structural optimization, regardless of the initial location, the Pt atom always locates on either the BA or BC site. Our results are in parallel with previous study [23, 29, 30]. It turns out that the Pt atom is more stable on the BC site than on the BA site. As exhibited in Table 1, the calculated binding energy is −3.88 eV at the BC site, on which the lengths for the Pt–Si and Pt–C bonds are 2.45 and 2.04 Å, respectively. At the BC site, bond length of Si–C near Pt atom is increased by about 0.06 Å with respect to metal-free nanotube and the corresponding bond lengths are nearly the same as those at the BA site, which is in agreement with previous study [6].

Upon Pt adsorption on SW defects in (8,0) SiCNT, eight stable configurations on each SW defect are investigated. As displayed in Fig. 4b, c, the Pt atom in SW-a nanotube prefers to adsorb on Si–Si bond in 5-7 ring fusion. On the other hand, Pt atom in the SW-c nanotube stays on seven-membered ring, which has four Si atoms. As presented in Table 1, the central bond in 7-7 ring fusion is increased by Pt adsorption. In addition, the length of this bond in Pt@SW-a structure is longer than Pt@SW-c one. The minimum distance (d_{min}) between Pt atom and Si atom in SW-a and SW-c structures are 2.22 and 2.34 Å, respectively. Moreover, Pt atom and C atom in SW-c structure are closer to each other than SW-a structure. Due to adsorption and accruing sp^3 hybridization, θ_p of C and Si atoms in 5-7 ring fusion in SW-a are larger than before coating. According to data in Table 1, θ_p for C and Si atoms in SW-c become longer and smaller than before adsorption, respectively. As a result, Pt atom is near to atom with high θ_p.

The adsorption or binding energy is defined as

$$E_b = E_{(Pt@SiCNT)} - E_{(SiCNT)} - E_{(Pt)},$$

where $E_{(Pt@SiCNT)}$, $E_{(SiCNT)}$, and $E_{(Pt)}$ are the total energy of the Pt adsorbed on a perfect or a defective SiCNT, the total energy of a perfect or a defective SiCNT, the total energy of the isolated Pt atom, respectively. As mentioned in Table 1, the binding energy of Pt atom on SW-a and SW-c structures are −5.65 and −5.61 eV, respectively. Interestingly, both are strongly exothermic. As a result, the Pt atom adsorbed on the Si–Si bond (Pt@SW-a configuration) is the most stable configuration. Hence, SW defects can enhance

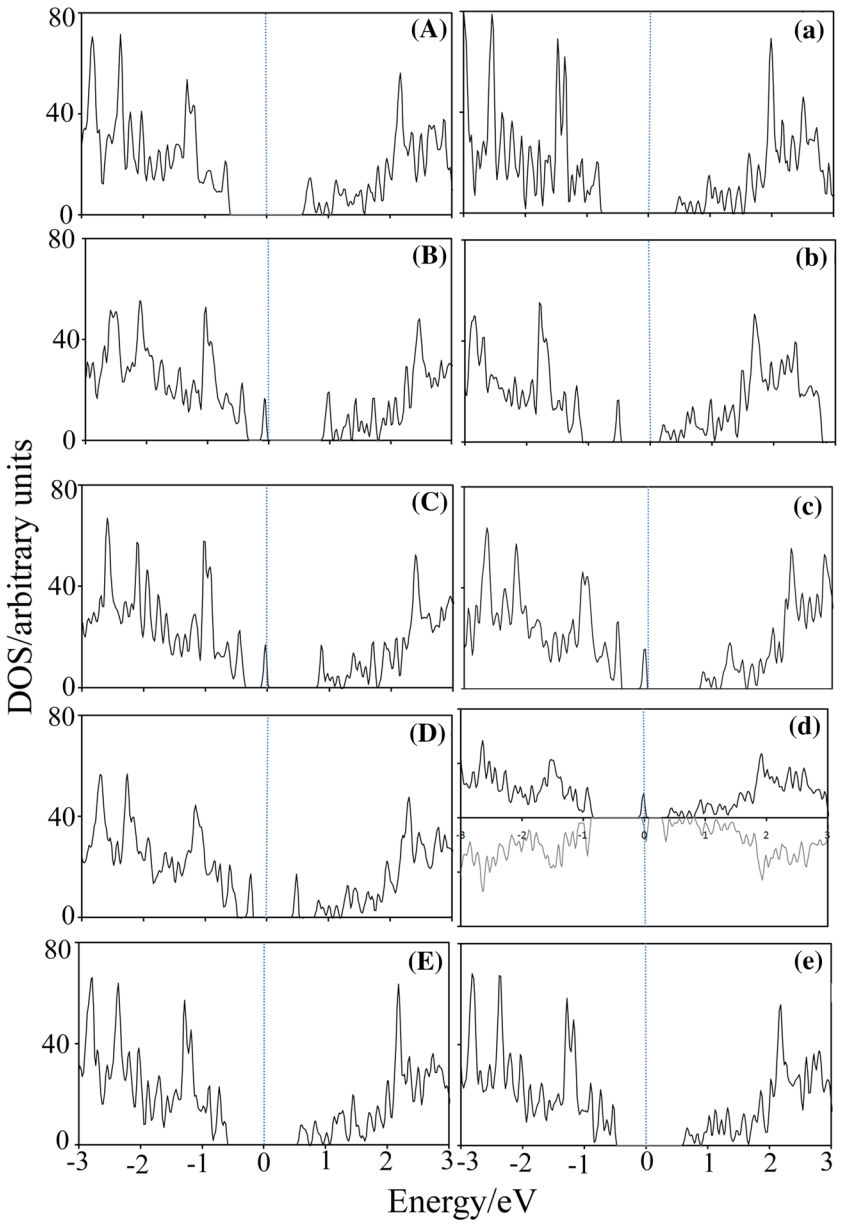

Fig. 3 Density of states (DOS) of a, **a** perfect SiCNT, **b** SW-c, **c** SW-a, **d** Si_V, and **e** C_V. Furthermore, the DOS of a **A** Pt@perfect, **B** Pt@SW-c, **C** Pt@SW-a, **D** Pt@Si_V, and **E** Pt@C_V. The DOS for majority-spin electrons are plotted *upward* and minority-spin *downward*. The Fermi level is set to zero and is indicated by the *dashed blue line* (color figure online)

the reactivity of the nanotube and the stability of the Pt adsorption.

In the case of atom vacancy, four different positions for atom adsorption are investigated, including the top site of the UA, the hollow sites of the five- and nine-membered ring, and the bridge site over new bond. Our calculations showed that, the most favorable adsorption site in carbon and silicon vacancy is on the nine-membered ring as shown in Fig. 4d, e. Furthermore, Pt atom is closer to UA in Si_V structure rather than C_V structure. After Pt adsorption, the length of the new bond is increased and there is no UA in the vacant structures. Based on binding or adsorption energy, Pt@C_V structure has 6.3 meV/atom lower binding energy than Pt@Si_V structure. The absolute binding energies of Pt on SW and vacancy defects in our systems are in the range of 5.61–6.66 eV, which are greater than the values were obtained by scientists in CNT, BNNT, and GaNNT structures [23, 30, 36]. It is noted that Pt atom on the defective SiCNT has a more binding energy respect to cohesive energy of Pt bulk (5.84 eV/atom) [37]. As a result, Pt atom does not suffer from clustering problem. Therefore, the Pt atom on a vacancy defect of SiCNT could have extra benefits as a new type of catalyst, gas sensor, and reversible hydrogen sorption.

Figures 3 and 5 and Tables 1 and 2 indicated that the calculated electronic band structure and DOSs of the perfect and the defective (8,0) SiCNT before and after Pt atom adsorption. Upon Pt adsorption on pristine, two "impurity states" appear above and below Fermi level by which direct band gap is decreased to 1.0 eV. The same results

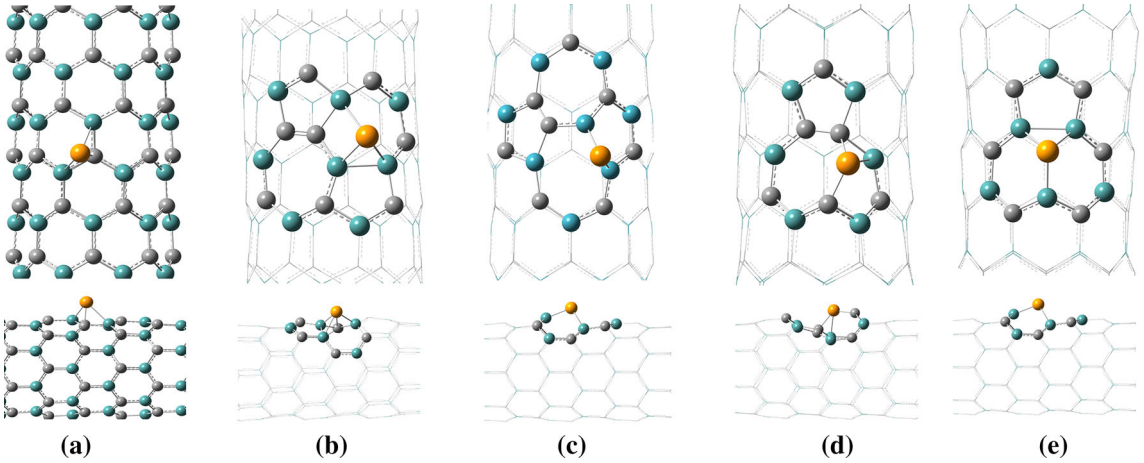

Fig. 4 The most stable configuration of adsorption of Pt atom on **a** perfect (8,0) SiCNT, **b** SW-c, **c** SW-a, **d** Si_V, and **e** C_V structures. *Gray*, *dark turquoise*, and *orange colors* represent carbon, silicon, and platinum atoms, respectively (color figure online)

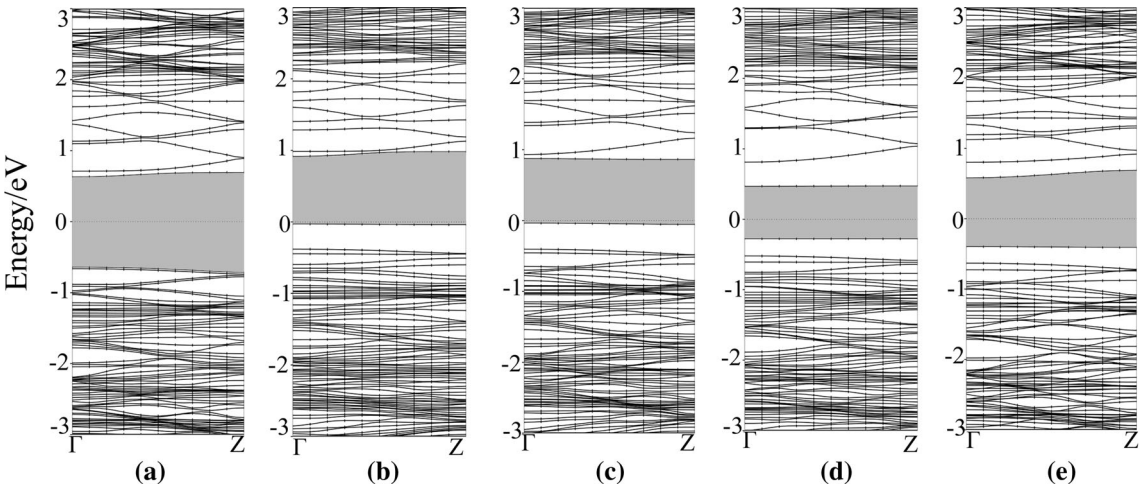

Fig. 5 Electronic band structure along high symmetry points for **a** Pt@perfect, **b** Pt@SW-c, **c** Pt@SW-a, **d** Pt@Si_V, and **e** Pt@C_V. The gap between valence and conduction bands is distinguished by *gray color*

were also observed in Pt on CNT, BNNT, and GaNNT [36, 38, 39]. Moreover, energy levels in Pt@perfect become non-flat and energy levels delocalized. When Pt atom is adsorbed on SW-c structure an "impurity state" appeared below CBM. In addition, the Fermi level and CBM are shifted to VBM and higher energy, respectively. As a result, the band gap between VBM and CBM are increased. Moreover, in Pt@SW-a an "impurity state" above Fermi level appeared, so the band gap is decreased. Compared with Si_V, the electronic structure of Pt@Si_V is dramatically changed. The band gap is changed to 0.54 eV. Moreover, Pt atom on C_V structure produces an "impurity state" above the Fermi level. Therefore, the value of the band gap in Pt@C_V is more than C_V structure. In the Pt@SW-a structure and Pt@Si_V structure, the energy levels of VBM and CBM become quite flat and energy levels localized with respect to metal-free SW-a and Si_V nanotube. It is worth mentioning that all the nanotubes with atomic Pt show paramagnetic ordering.

Turning now to the chemical nature of the interaction between Pt atom and nanotubes, the calculated charge transfer of Pt (ΔQ_{Pt}) on perfect and defective structure obtained by Löwd in charge analysis are listed in Tables 1 and 2. It is notable that a negative value for ΔQ_{Pt} indicated that the Pt atom lose electron density. Upon Pt atom adsorption, the *s*-orbital (*d*-orbital) of Pt atom lose (gain) electrons; therefore, is classified as Dewar coordination [31]. Nevertheless, both of the *s*-orbital and *d*-orbital lose some charge in Pt@Si_V. Interestingly, it can be inferred from the charge transfer that the Pt atom in the perfect and

vacancy systems is in a cationic state and can accept electrons from other molecules such as molecular hydrogen, while Pt atom in the SW systems is in an anionic form and can donate electrons to other molecules. When the Pt atom is adsorbed to the surface of perfect and defective SiCNT, there is a certain amount of charge transferred between the metal atoms and the nanotube. As shown in Table 2, UAs in C_V and Si_V structures gain and lose charge, respectively. It seems that, electronegativity plays a crucial role for these charge transfers. After Pt adsorption, these atoms in C_V and Si_V lose 0.65e and gain 0.53e, respectively. It is noticed that high charge transfer is associated with strong adsorption effect. The evolution of absolute charges on the UA and Pt atoms during adsorption indicated a stronger electrostatic interaction, leading to the bond formation between them.

Conclusions

Using spin-polarized DFT, we have studied pristine, SW defects, and vacancy defects of SiCNT before and after atomic Pt adsorption. It is noteworthy that the structures with and without Pt atom remain semiconductor with a direct band gap. Among all the structures, magnetic behavior has been observed only in Si_V structure. In the perfect structure, regardless of the initial location, the Pt atom prefers to stay on axial Si–C bond. In addition, SW-a structure is a desirable adsorbent rather than SW-c structure. Based on binding energy, the most favorable system for Pt adsorption is the C_V structure. It is worthy of note that the large binding energy between the nanotubes with vacancy defects and Pt atom prevents clustering of the dopants. Moreover, Pt atom on perfect and vacancy defects is in a cationic state, while on the SW structure is in an anionic state. Hence, in the future studies, the Pt atom on a vacancy defect of SiCNT could have extra benefits as a new type of catalyst, gas sensor, and for hydrogen storage.

Computational details

Spin-polarized DFT calculations, implemented in the QUANTUM ESPRESSO package [40] are performed on (8,0) SiCNT. A super cell containing 128 atoms is chosen and a plane-wave basis set with a cutoff value of 600 eV is used in combination with Vanderbilt ultrasoft pseudopotentials [41] and the Perdew–Burke–Ernzerh of (PBE) [42] exchange–correlation functional within the generalized gradient approximation (GGA). To determine the equilibrium structure of the systems, full relaxation without any constraints is performed until the acting forces on any atom are less than 0.001 eV/Å. In addition, the Brillouin-zone integration is performed with a $1 \times 1 \times 7$ Monkhorst-Pack k-points mesh [43]. In order to ensure negligible interaction between the system and its images in neighboring cells, a large super cell parameter of 25 Å in x and y directions is chosen. Furthermore, we have measured the pyramidalization angles at selected atom sites using Haddon's π orbital axis vector (POAV) method [44]. The pyramidalization angle (θ_p) is a measure of the degree of sp^3 hybridization of an atom, defined as ($\theta_{\sigma p} - 90°$), where $\theta_{\sigma p}$ is the angle between σ and π bonds. For $\theta_p = 0°$, the hybrid is sp^2 as in a flat graphene [44, 45] and for $\theta_p = 19.5°$ the atom is sp^3 hybridized as in methane.

Acknowledgments Computations were performed on the GPC supercomputer at the SciNet HPC Consortium. SciNet is funded by: the Canada Foundation for Innovation under the auspices of Compute Canada; the Government of Ontario; Ontario Research Fund-Research Excellence; and the University of Toronto. Further, we are grateful to Sanandaj Branch, Islamic Azad University Council for the financial support of this research.

References

1. Xi G, He Y, Wang C (2010) Chem Eur J 16:5184
2. Zhao M, Xia Y, Li F, Zhang R, Lee S-T (2005) Phys Rev B 71:085312
3. Mpourmpakis G, Froudakis GE, Lithoxoos GP, Samios J (2006) Nano Lett 6:1581
4. Wu R, Yang M, Lu Y, Feng Y, Huang Z, Wu Q (2008) J Phys Chem C 112:15985
5. Zhang W, Zhang F, Zhang Z, Lu S, Yang Y (2010) Sci Chin Phys Mech Astron 53:1582
6. Zhao J-X, Ding Y-H (2008) J Phys Chem C 112:2558
7. Sun X-H, Li C-P, Wong W-K, Wong N-B, Lee C-S, Lee S-T, Teo B-K (2002) J Am Chem Soc 124:14464
8. Stone AJ, Wales DJ (1986) Chem Phys Lett 128:501
9. Pan BC, Yang WS, Yang J (2000) Phys Rev B 62:12652
10. Orellana W, Fuentealba P (2006) Surf Sci 600:4305
11. Bettinger HF (2005) J Phys Chem B 109:6922
12. An W, Wu X, Yang J, Zeng X (2007) J Phys Chem C 111:14105
13. Jalili S, Akhavan M, Schofield J (2012) J Phys Chem C 116:13225
14. Jalili S, Molani F, Akhavan M, Schofield J (2014) Physica E 56:48
15. Wang Z, Gao F, Li J, Zu X, Weber WJ (2009) J Appl Phys 106:084305
16. Wang X, Liew K (2012) J Phys Chem C 116:26888
17. Baierle R, Piquini P, Neves LP, Miwa R (2006) Phys Rev B 74:155425
18. Mao Y-L, Yan X-H, Xiao Y (2005) Nanotechnology 16:3092
19. Zhang J-M, Wang S-F, Chen L-Y, Xu K-W, Ji V (2010) Eur Phys J B 76:289
20. Chen YK, Liu LV, Tian WQ, Wang YA (2011) J Phys Chem C 115:9306
21. Jalili S, Molani F, Schofield J (2013) Can J Chem 91:1
22. Banerjee S, Nigam S, Pillai C, Majumder C (2012) Int J Hydrogen Energy 37:3733
23. Wu X, Yang J, Zeng XC (2006) J Chem Phys 125:044704
24. Tian WQ, Liu LV, Wang YA (2006) Phys Chem Chem Phys 8:3528
25. Yeung CS, Liu LV, Wang YA (2008) J Phys Chem C 112:7401

26. Li XM, Tian WQ, Huang X-R, Sun C-C, Jiang L (2009) J Mol Struct Theochem 901:103
27. Li K, Wang W, Cao D (2011) Sens Actuators B 159:171
28. Zhang X, Dai Z, Wei L, Liang N, Wu X (2013) Sensor 13:15159
29. Chen G, Kawazoe Y (2006) Phys Rev B 73:125410
30. Park Y, Kim G, Lee YH (2008) Appl Phys Lett 92:083108
31. Gali A (2006) Phys Rev B 73:245415
32. Dinadayalane TC, Leszczynski J (2007) Chem Phys Lett 434:86
33. Li Y, Zhou Z, Golberg D, Bando Y, von Ragué Schleyer P, Chen Z (2008) J Phys Chem C 112:1365
34. Lin T, Wei-De Zhang, Huang J, He C (2005) J Phys Chem B 109:13755
35. Lu X, Chen Z, Schleyer PvR (2005) J Am Chem Soc 127:20
36. Chen G-X, Zhang Y, Wang D-D, Zhang J-M (2010) Phys E 43:22
37. Kittel C (2005) Introduction to solid state physics, 8th edn. Wiley, New York
38. Wu X, Zeng XC (2006) J Chem Phys 125:44711
39. Tabtimsai C, Ruangpornvisuti V, Wanno B (2013) Phys E 49:61
40. Giannozzi P, Baroni S, Bonini N, Calandra M, Car R, Cavazzoni C, Ceresoli D, Chiarotti GL, Cococcioni M, Dabo I (2009) J Phys Condens Matter 21:395502
41. Vanderbilt D (1990) Phys Rev B 41:7892
42. Perdew JP, Burke K, Ernzerhof M (1996) Phys Rev Lett 77:3865
43. Monkhorst HJ, Pack JD (1976) Phys Rev B13:5188
44. Haddon R (2001) J Phys Chem A 105:4164
45. Haddon R (1990) J Am Chem Soc 112:3385